CHAPTER 2 LITERATURE REVIEW

2.1 The titanium aluminides

2.1.1 Introduction

Titanium aluminide (TiAl) is an intermetallic compound. It is lightweight (with an approximate density of 3.8 g/cm³) and resistant to oxidation and heat but TiAl suffers from low ductility. It is used in several applications, including automobiles and aircrafts. Developments of TiAl-based alloys began approximately in the 1970s and have been used in the automobile and aircraft applications since approximately 2000[6].

Titanium aluminide can be classified into three major intermetallic compounds: γ-TiAl, α_2-Ti$_3$Al and TiAl$_3$. Among the three, γ-TiAl has received the most attention and is used in most applications. γ-TiAl has excellent mechanical properties and oxidation and corrosion resistance at elevated temperatures (550-750°C) which makes it a possible replacement for the traditional Ni-based superalloy components used in aircraft turbine engines [4]. Table 1.1 presents several physical and mechanical properties of such alloys compared with those of the common commercial titanium and nickel alloys. The data show that titanium aluminides significantly exceed titanium alloys in several properties and are comparable with nickel alloys. Specifically, modulus of elasticity and operational temperatures are higher than those of commercial titanium alloys. TiAl-based alloys have a strong potential to increase the thrust-to-weight ratio in aircraft engines. This is especially the case for engines with low-pressure turbine blades and high-pressure compressor blades. These are traditionally made of Ni-based superalloys which is nearly twice as dense as TiAl-based alloys [7].

Table 2.1 A comparison of the properties of aluminides and the nickel-based titanium alloys [10]

Properties	Ti(base)	Ti$_3$Al	TiAl	High-temperature nickel alloy
Density, g/cm^3	4.5	4.15-4.7	3.76	8.3
Young's modulus (Gpa)	110-96	145-110	176	206
Operational temperature:				
by admissible creep, ºC	550	800	1050	1100
by admissible oxidation, ºC	600	650	1050	1100
Ductility at 20ºC, %	20	2-5	1-2	3-5
Ductility at operational temperature, %	Over 20	5-8	7-12	10-20

2.1.2 Crystal structures of titanium aluminides

The crystal structures of titanium aluminide family are classified into three main compounds (Figure 2.1), as follow:

- Ti$_3$Al-based: the crystal is an ordered α_2-phase of the D0$_{19}$ structure with a hexagonal symmetry (hP8) and lattice parameters of a$_{ord}$ = 2a$_{disor}$ = 0.58 nm; c$_{ord}$ = 0.48 nm. The latter derives from the A$_3$ type structure but presents a long-range order only in the direction perpendicular to the c-axis.

- TiAl-based: the crystal is a γ ordered structure until the melting point with an L1$_0$ type face-centered tetragonal (tP4) structure consisting of atomic layers perpendicular to the c-axis.

- TiAl$_3$-based ordered structure: based on the D0$_{22}$ structure (tI8). This structure is related to two L1$_2$ type unit cells stacked along the c-axis with an antiphase boundary of 1/2[110](001) type at every other (0 0 1) plane.

The crystal structure has a significant capacity to improve the ductility properties by heat treatment which transforms the structure from D0$_{22}$ structure into higher symmetry

L1$_2$ structure. Additions of Fe or Cu (approximately 10 at.%) can promote the transformation although ductility is not much improved.
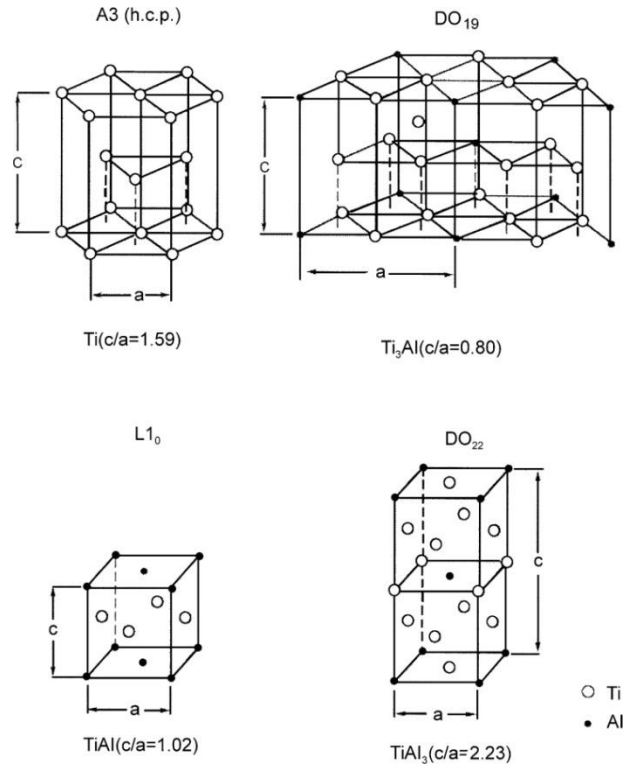

Figure 2.1 Crystal structures of the four model phases (Ti, Ti$_3$Al, TiAl and TiAl$_3$) in the Ti-Al system [11]

Previous research on TiAl-based alloys focused on the effects of composition (35 to 65 at.% Al) on structure which is either a mixture of the γ(L1$_0$) and (α$_2$ (D0$_{19}$) phases or the γ-phase [12] . For γ alloys rich in titanium, the primary phase that crystallizes from the liquid is β. The solidification path is as follows: L → [β] + L → [β + α] → [α] → [α + γ] → [α$_2$ + γ]. Upon cooling, the phase becomes unstable and transforms into α phase. With further solid state cooling, α phase becomes unstable and orders into α$_2$ phase at approximately 1117 $^\circ$C [13].

For alloys in the range of 49 and 55 at.%Al, the primary phase is α. The solidification and solid state transformations of the alloys in this range can be summarized by L → [α] + L → [α] + γ → γ. The γ phase has a lamellar structure.
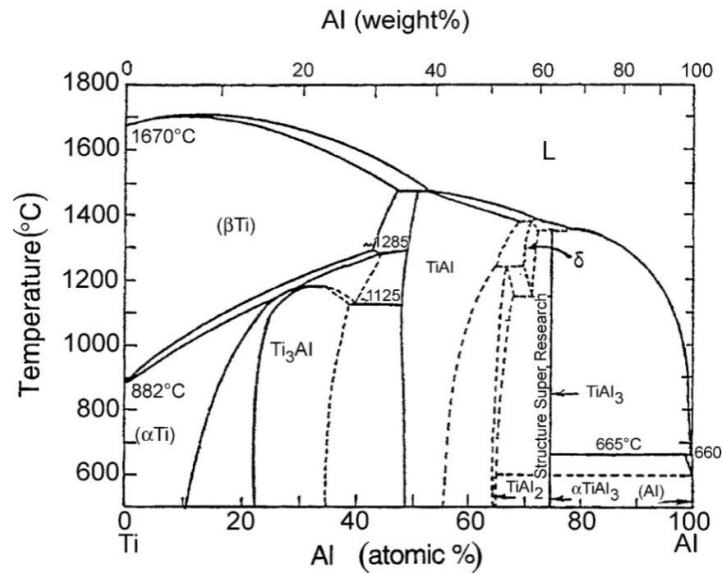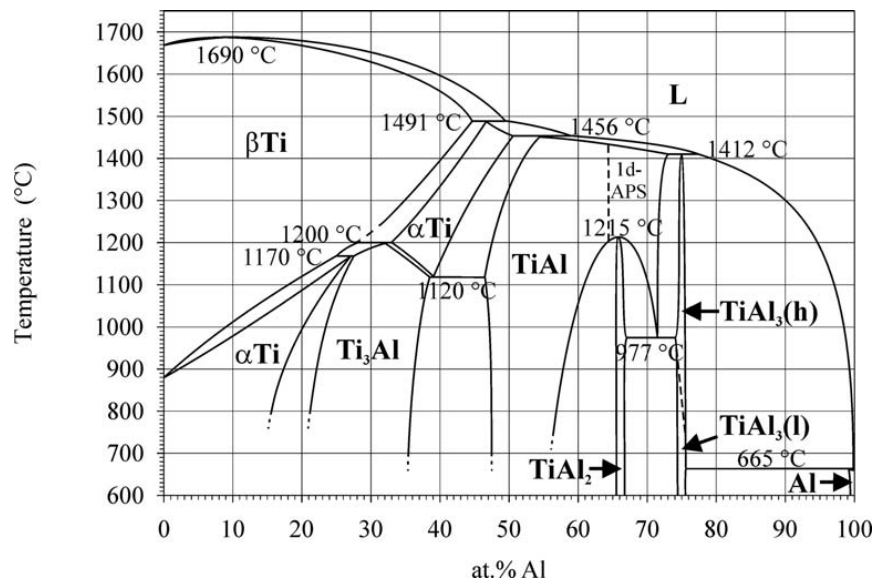

Figure 2.2 Ti–Al phase diagram [12]

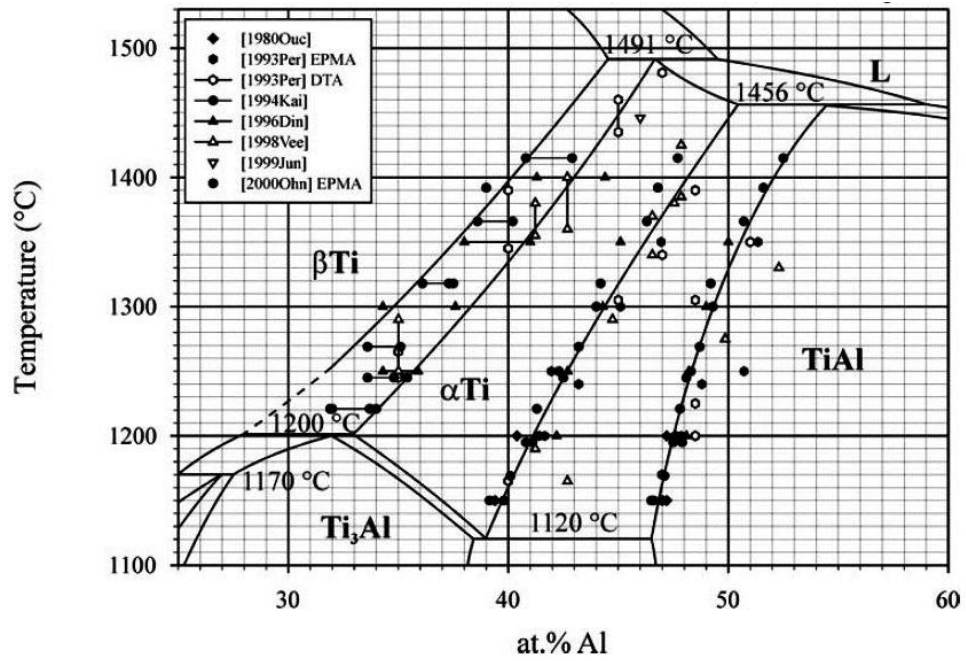**Figure 2.3** Ti-Al system according to the current assessment [14]

Figure 2.4 A section of the binary Ti-Al phase diagram according to the assessment
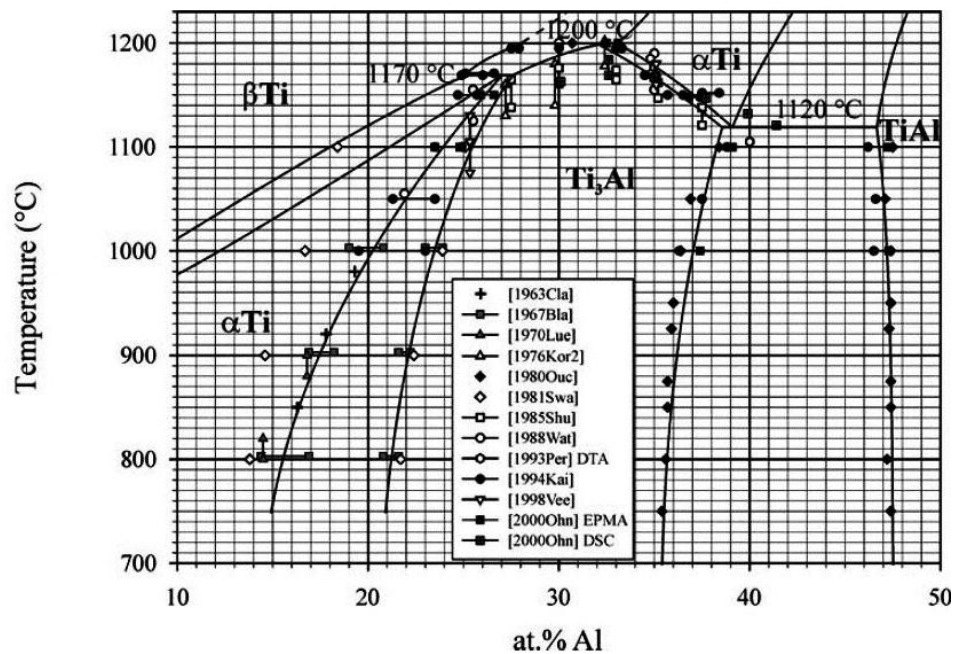
of Schuster and Palm [14]

Figure 2.5 A section of the binary Ti-Al phase diagram according to the assessment
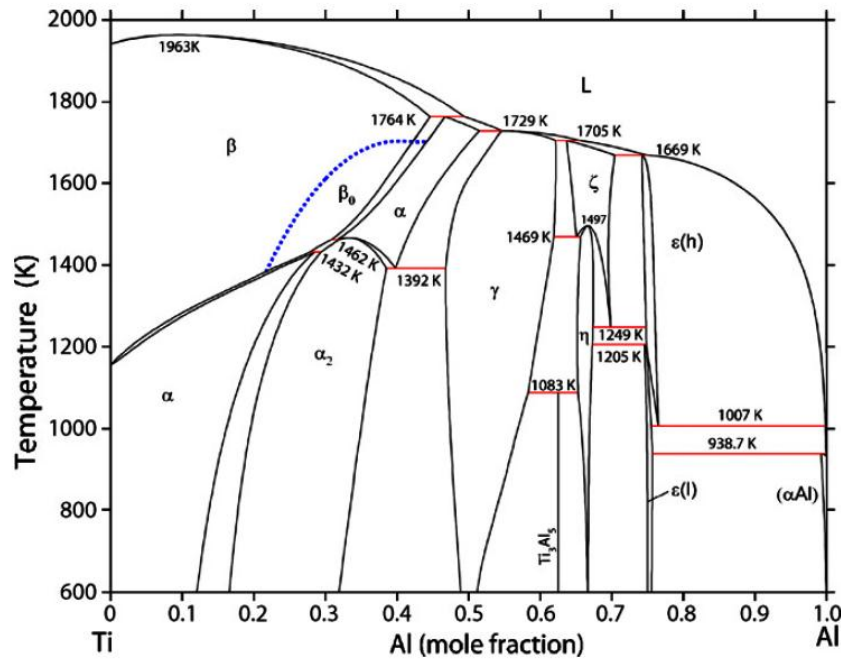
of Schuster and Palm [14]

Figure 2.6 Ti-Al systems according to the present thermodynamic description [14]

Various Ti-Al binary phase diagrams, based on the results of previous work, are shown in Figures 2.3, 2.4, 2.5 and 2.6. These figures show the phase diagrams that were produced by Schuster and Plam [14] (Figure 2.3, 2.4 and 2.5) and Witusiewicz et al. [15], respectively. The two phase diagrams are nearly identical, yet they exhibit a difference in order for Al compositions greater than 60 at.%. The diagram by Witusiewicz et al. [15] identified the Ti_3Al_5 and $Ti_{2+x}Al_{5-x}$ phases. Both of the presented diagrams confirm the peritectic reaction $L+\beta \rightarrow \alpha$, which were not accepted in the assessment of Murray [12]. Figures 2.3, 2.4, 2.5 and 2.6 confirmed that the peritectic reaction in both phase diagrams includes the first reaction of $L+\beta \rightarrow \alpha$ and the second reaction of $\beta + \alpha_2 \rightarrow \alpha$. Moreover, Schuster and Plam [14] concluded that the Al-rich alloys (containing 63-73 at.% Al), which were quenched from a temperature of approximately 1215°C, yielded a unique structure; a one-dimensional antiphase domain

structure (1d APS) was revealed, designated as the phases of Ti_5Al_{11}, γ_2, Ti_2Al_5 or long period superstructures.

2.1.3 Microstructures of the titanium aluminides

The two phase-based titanium aluminides at an approximate composition of Ti–(45–49) Al can be classified into four groups designated as near γ, duplex, nearly lamellar and fully lamellar microstructures. These structures are formed by annealing temperature at the temperatures T_2, T_3, T_4 and T_5 (Figure 2.7) [13]. The near γ microstructure is generally non-uniform, consisting of coarse γ grains and stringers of fine γ grains pinned by α_2 particles (Figure 2.8a). The duplex microstructure contains equal volume fractions of α and γ phases. The competitive growth between α and γ grains leads to a fine microstructure (Figure 2.8b).
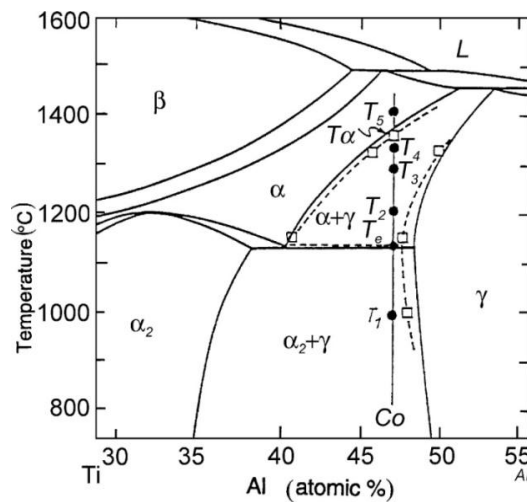

Figure 2.7 A section of the Ti–Al phase diagram [16]

The near lamellar microstructure consists predominantly of coarse α lamellar grains with minor amounts of fine γ grains. Finally, the totally lamellar microstructure is

composed of alternating plates of α_2 and γ which have the usual crystallographic relationships. The significant diffusivity that occurs at high temperatures leads to the rapid growth of α grain (Figure 2.8c).
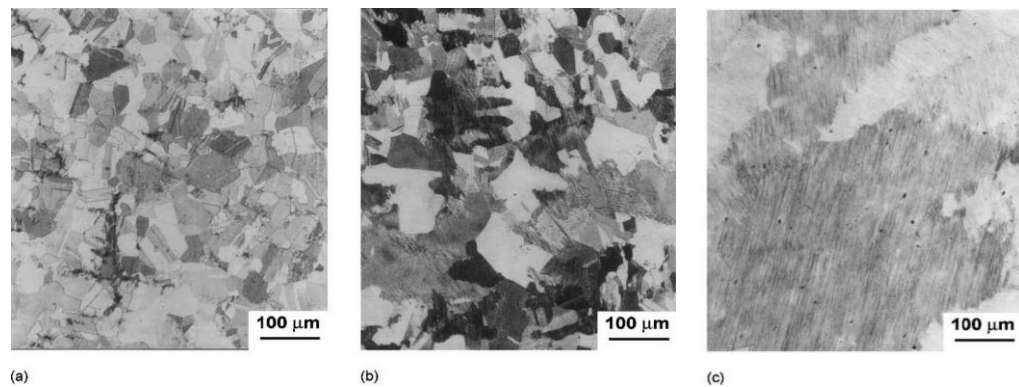

Figure 2.8 Microstructures of forged Ti–47Al–1V–1Cr–2.5Nb two-phase γ alloy after the following heat treatments: (a) T_2, (b) T_3, and (c) T_5 [16]

2.2 Gamma titanium aluminide (γ-TiAl)

2.2.1 General properties

Gamma titanium aluminide alloys are promising candidate materials for use in components of aerospace or automotive engines which are used under high temperatures and mechanical loads due to their high temperature properties [4] and attractive combination of low density (approximately 3.8 g/cm^3), high melting temperature, good oxidation and burn resistance, high modulus and strength retention at elevated temperatures, and good creep properties [17, 18]. However, the limiting properties for the service applications of these alloys include poor ductility at room temperature, low fracture toughness, fast fatigue crack growth rates, and low oxidation resistance above 800°C [17,18]. Further, mechanical properties of gamma TiAl are

associated with both chemical composition of alloying elements and the microstructure. The alloys can be used to develop desired mechanical properties by alloying element additions as well as changes in microstructure by heat treatment for improved mechanical properties and a trade-off between fracture toughness and ductility [18]. The composition of γ-TiAl-based alloys is maintained between 45-51 at.% Al with 1-10 at.% ternary additions of alloying elements. Generally, ternary alloying element additions yield improved structures and properties such as refinements of grain sizes, improvements in high-temperature properties, and increases in ductility at room temperature. Alloying elements that yield significantly improved properties include V, Mn, Mo and Cr for promoting room temperature ductility [17,19,20]; Si, Ni, and Ta for improving oxidation properties; Ta, C, N, W, and Si for improving the creep resistance; and Nb for improving fatigue strength. Finally, grain size refining is effected by additions of W and/or B.

2.2.2 Constitution of γ-titanium Aluminides Alloys

Two-phase diagrams are presented in Figure 2.9. The first diagram, shown in figure 2.9(a), is a binary Ti–Al phase diagram as proposed by McCullough et al. [21] and reasonably reflects the phase equilibria in the concentration range of 40–55 at% Al when small deviations in the solubility lines are disregarded. Figure 2.9 (b) is a quasi-binary section of the ternary Ti-Al-Nb diagram for a Nb concentration of 8 at%, as determined by Zhang et al. [22] in comparison to the binary phase diagram calculated by Okamoto [23].
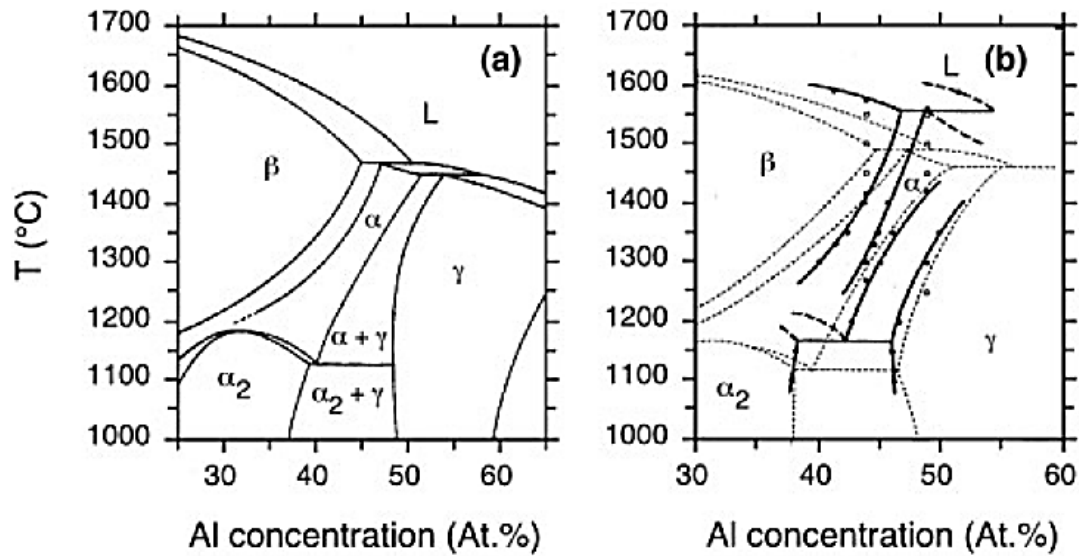
Figure 2.9   Constitution of the Ti-Al-alloys. (a) Binary Ti–Al phase diagram and (b)

Ternary Ti-Al-Nb diagram for a Nb concentration of 8 at%.[21]

The crystal structures of the γ-titanium aluminide alloys are presented in Figure 2.9 (a)

and (b) and contain several intermetallic phases in three types known as: (1) the

hexagonal α_2-Ti$_3$Al phase, with the Strukturbericht designation DO$_{19}$, prototype Ni$_3$Sn,

Pearson symbol hP8, space group P6$_3$/mmc, and lattice parameters a=0.5782 nm,

c=0.4629 nm (Figure 2.10 (a)); (2) the tetragonal γ-TiAl phase, with the Strukturbericht

designation L$_{10}$, prototype AuCu, Pearson symbol tP2, space group P4/mmm, and lattice

parameters a=0.4005 nm, c=0.4070 nm(Figure 2.10 (b)); and (3) the cubic high-

temperature B2 phase, with the Strukturbericht designation B2, prototype CsCl, Pearson

symbol cP2, and space group $Pm\bar{3}m$(Figure 2.10 (c)). [24]
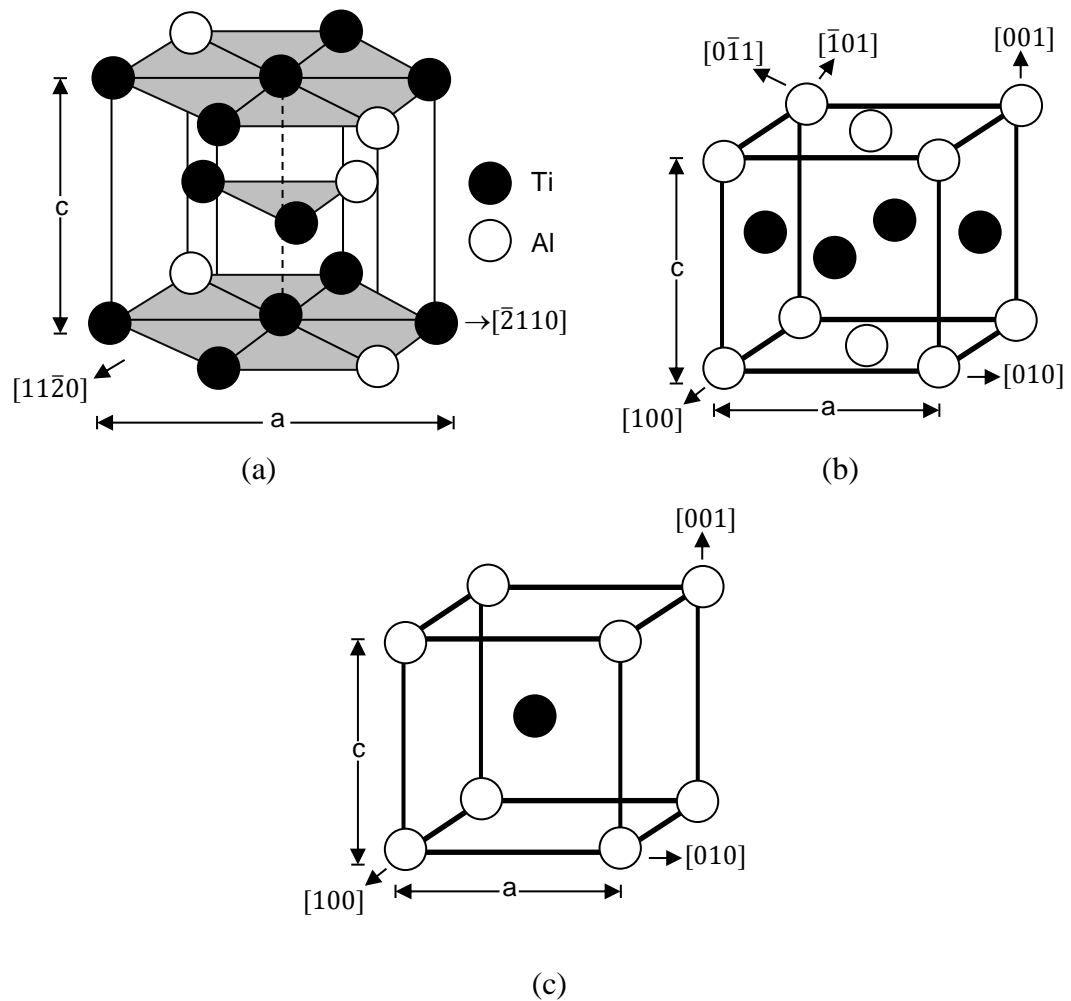
Figure 2.10 Crystal structures of the binary titanium aluminide phases [24].

The two phases of the gamma titanium aluminides that contain major fractions of γ-TiAl and minor fractions of α_2-Ti$_3$Al have been further investigated in light of a significant focus for engineering applications. Generally, the γ-TiAl phase possesses Al concentrations of 45–48 at% and thus solidifies peritectically, according to the phase diagram. Depending on the processing conditions and the composition, it is possible that as many as two peritectic reactions may occur. During ingot processing or casting, peritectic solidification often results in macroscopic columnar grains as well as a pronounced microsegregation of the alloying elements. Both of these features, as

observed in the cast microstructure, only can be removed with difficulty [25] and might be disadvantageous to the mechanical properties. The growth of columnar grains in preferential crystallographic orientations with respect to the heat flow direction can further result in strong solidification textures. The casting textures are particularly pronounced if grains of the hexagonal α solid solution solidify, as is the case for many engineering alloys [26].

Thus, the texture of cast alloy parts can be influenced by selecting different solidification paths, which can be achieved by incorporating relatively small variations in the alloy composition; this approach is used in the development of directional solidification processing [27]. In particular, complete solidification through the β phase without a peritectic reaction is possible for Al contents <45 at.%, and this approach is currently being investigated for the development of cast alloys [26].

After solidification, binary (TiAl) alloys pass through the single-phase field of the α solid solution, which decomposes upon further cooling according to the reactions α→α+γ→α$_2$+γ or α→α$_2$→α$_2$+γ [28]. The existence of this single phase high-temperature field is a characteristic feature of the γ-TiAl alloys in comparison to other intermetallic alloys. Similar to steels that have followed heat treatments in the austenite region, a variety of different phase transformations can occur upon cooling from the region or upon the application of subsequent heat treatments. These allow, in principle, a wide range of microstructures to be obtained [28].

The eutectoid transformation α→α$_2$+γ achieved upon cooling should also be mentioned, because it occurs in all engineering γ-TiAl alloys. The mechanism of this reaction

appears to be identical to the reaction α→α+γ, proceeding via the nucleation and growth of individual γ-lamellae. The occurrence of a discontinuous reaction, which evolves behind the moving interface, has not been observed until now [29]. For alloy compositions that deviate from the eutectoid composition, the volume fraction of the phase must increase abruptly, following the attainment of thermodynamic equilibrium, if the temperature falls below that of the eutectoid transformation. This can occur by the formation of new lamellae or by the growth of existing lamellae. The typically applied cooling rates, however, often do not allow thermodynamic equilibrium to be approached, and therefore, the obtained microstructures are not stable at the intended service temperatures (approximately 700°C). Thus, when selecting the processing conditions, an equilibration treatment or adequate cooling conditions must be taken into consideration.

In previous research, Appel et al. [8] reported that the alloy development in gamma titanium aluminides has emerged as a result of a number of alloy development programs for different processing routes and applications. The alloys can be described by the general composition of Ti-(45–48) Al-(0.1–10)X (at.%), with X designating the elements Cr, Nb, V, Ta, Mo, Zr, W, Si, C, and B. Generally, for the compositions mentioned above, the α_2 phase is present with a volume fraction up to 20%, while the remainder is in the γ phase. The candidate alloying elements for additions into gamma titanium aluminides include both metallic and non-metallic elements. Additions of metals elements that form solid solutions affect the properties of γ-TiAl, such as the planar defect energies or the diffusion coefficient. However, additions of non-metallic elements promote the formation of a third phase by precipitation hardening or grain

refinement during casting, by stabilization of the microstructure against grain growth, or by the decomposition of transient phases into fine structures. In considering the influence of alloying additions on the intrinsic properties, the focus of previous research has been in the areas of solubility in the γ phase, the partitioning of the alloying elements between the α_2 and the γ phases, and the occupation of the alloying element on the two sublattices of the γ phase. Both Hao et al [30, 31] have shown that the lattice occupancy of different alloying elements is related to the boundaries of the ($\alpha_2+\gamma$) two-phase field in the respective (Ti-Al-X, with X=Nb, Ta, V, Cr, Mn, Fe or Ga) systems. For TiAl alloys, the results show that Zr, Nb and Ta atoms invariably occupy the Ti sites, while Fe, Ni, Ga and Sn atoms occupy the Al sites; overall, the alloy composition has no significant influence on the site preference. For Ti_3Al alloys, Ga and Sn atoms occupy the Al sites, while V, Cr, Mn, Zr, Nb, Mo and Ta atoms occupy the Ti sites; in particular, in this case, the site preference of V, Cr, Mn and Mo in TiAl alloys is different from that in Ti_3Al. It has been suggested that, in the order of increasing strength of stabilization at $900^{o}C$, V, Nb and Ta stabilize the α_2 phase, whereas Cr, Mn, Fe and Ga stabilize the γ phase.

Kainuma et al. [32] reported intriguing results from their study on the phase equilibria between α, α_2, β and γ phases in the Ti–Al-based ternary systems (Ti-Al-X system) at 1000, 1200 and 1300°C. They successfully identified the partitioning coefficients between different phases which established that almost all the elemental additions (except Zr) tended to partition into the β phase rather than into the α, α_2 or γ phase; however, Zr mostly partitioned into the γ phase. Additionally, with respect to the equilibrium state between the α_2 and the γ phases, V, Cr, Mo, Ta and W partitioned into

the α_2 phase rather than into the γ phase, whereas Mn, Fe, Co, Ni, Cu and Zr tended to concentrate within the γ phase. When focusing only on the results from 1200°C (Figure 2.11), it can be clearly seen that the alloying elements Zr, Nb and Ta are exceptional in the sense that they are soluble in higher concentrations in the γ phase; further, in the case of Nb, the solubility is as high as approximately 9 at.% at 1200°C, which was confirmed in isothermal sections of different ternary Ti-Al-X systems, presented in Figure 2.12 and 2.13.[32].
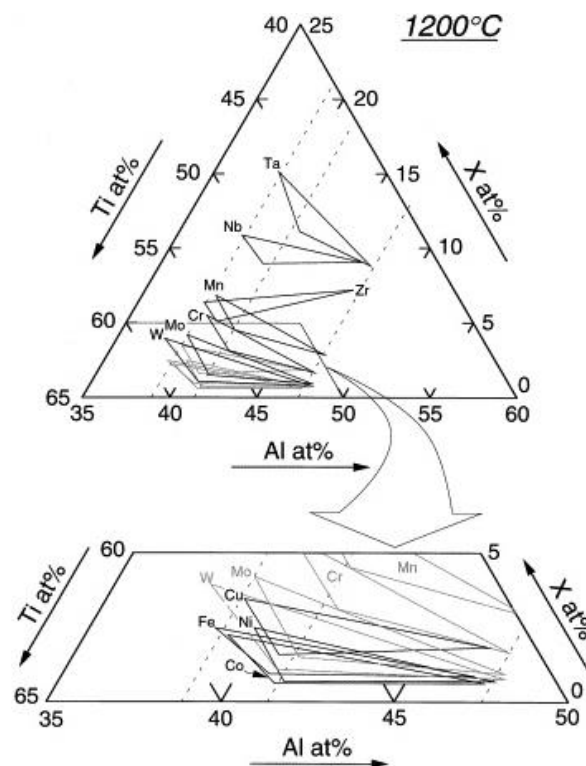
Figure 2.11 Positions of the $\alpha+\beta+\gamma$ three-phase triangles at 1200°C in the

Ti–Al–X ternary systems [32]

(a)

(b)

(c)

Figure 2.12 Phase equilibria in the Ti–Al-based ternary systems: (a) the Ti-Al-Zr,

(b) Ti-Al-Nb, and (c) Ti-Al-Ta systems, at 1000, 1200 and 1300°C [32]

Figure 2.13 Phase equilibria in the Ti–Al-based ternary systems: (a) the Ti-Al-Cr, and (b) Ti-Al-Mo systems, at 1000, 1200 and 1300°C [32]

Figure 2.14 Calculated isothermal section of the Ti-Al-Nb system at 700 °C according to the most recent thermodynamic re-evaluation conducted by Witusiewicz et al. [33]

Table 2.2 Phase designations in the isothermal section of the Ti-Al-Nb system

at 700°C [33]

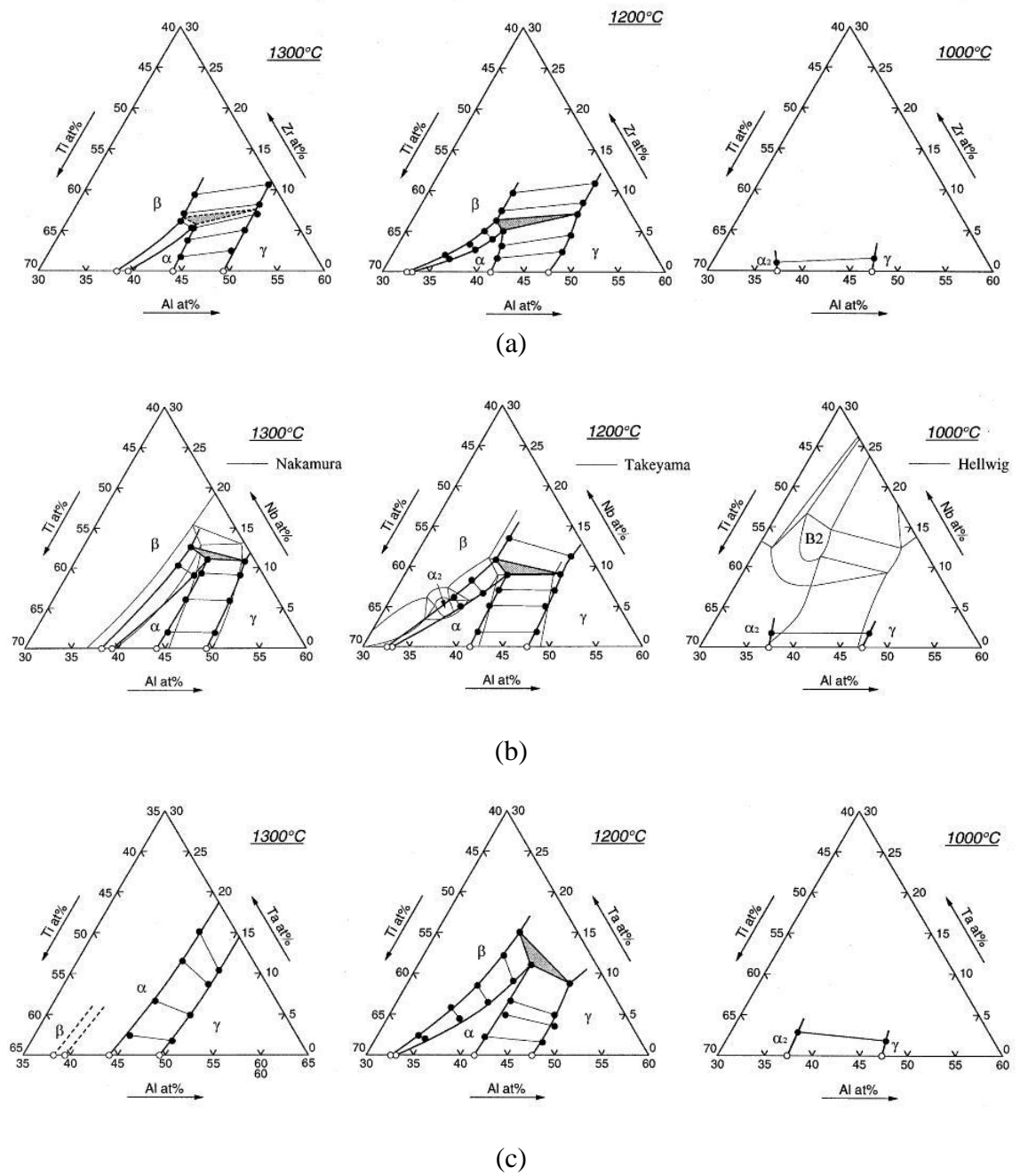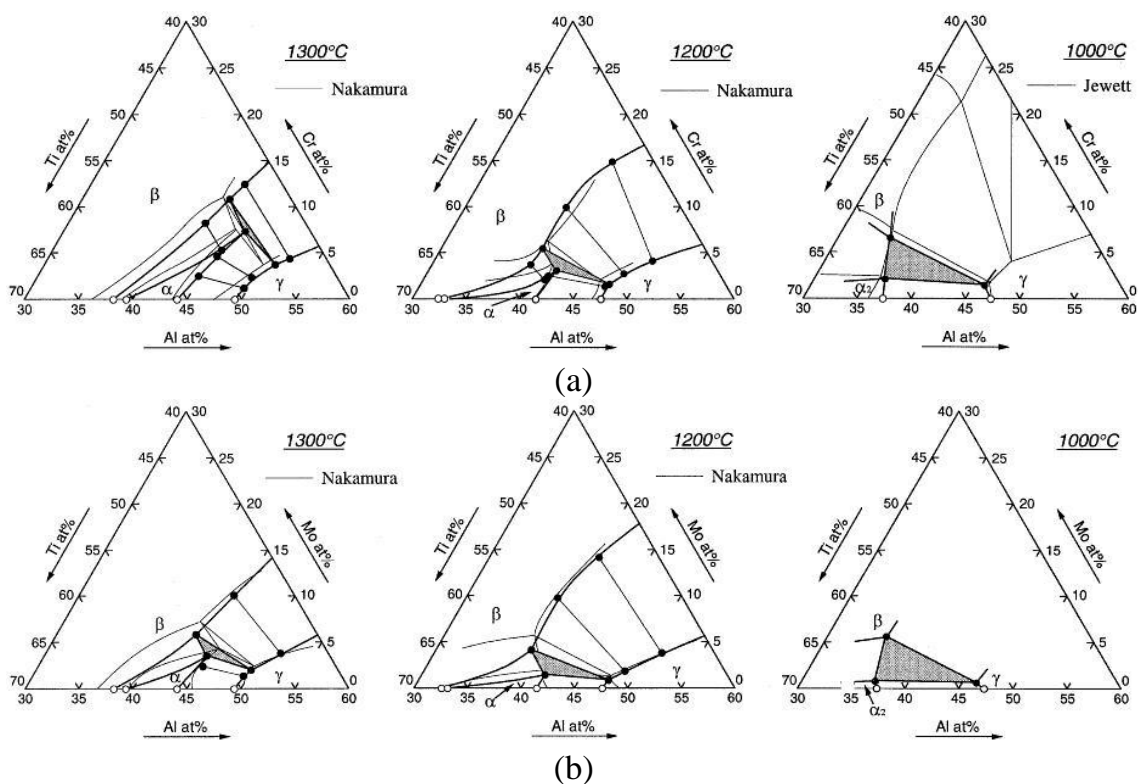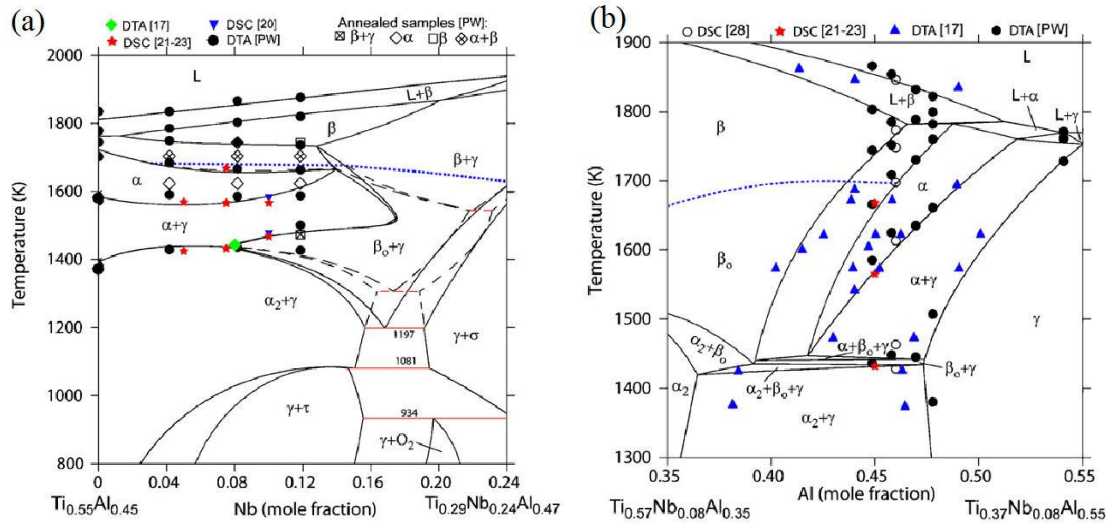| Designation	Pearson symbol	Space group	Strukturbericht designation
Al	cF4	$Fm\,\bar{3}m$	A1
α, α-Ti	hP2	$P6_3/mmc$	A3
β, β-Ti	cI2	$Im\,\bar{3}m$	A2
α_2 (Ti$_3$Al)	hP8	$P6_3/mmc$	D0$_{19}$
γ (TiAl)	tP4	P4/mmm	L1$_0$
O$_2$ (Ti$_2$AlNb)	oC16	Cmcm	
τ (Ti$_4$Al$_3$Nb), ω$_0$	hP6	$P6_3/mmc$	B8$_2$
δ (Nb$_3$Al)	cP8	$Pm\,\bar{3}n$	A15
σ (Nb$_2$Al)	tP30	$P4_2/mmm$	D8$_b$
Ti$_3$Al$_5$	tP32	P4/mbm	
η (TiAl$_2$)	tI24	$I4_1/amd$	
ε (l) (TiAl$_3$ (I))	It32	$I4/mmm$	

Figure 2.15 Calculated vertical sections close to the Al-Ti side of the Al-Nb-Ti

system according to the re-evaluation carried out by Witusiewicz et

al. [33]: (a) the isopleth for 45 at.% Al and (b) the isopleth for 8at.% Nb.

The dotted lines show the order-disorder transformation of the β-phase.

Table 2.3 Phase designations in the vertical sections close to the Al-Ti side of

Al-Nb-Ti system phase diagram [33]

Designation	Pearson symbol	Space group	Strukturbericht designation
α, α-Ti	hP2	$P6_3/mmc$	A3
β, β-Ti	cI2	$Im\,\bar{3}m$	A2
$β_0$	cP2	$Pm\,\bar{3}m$	B2
$α_2$ (Ti$_3$Al)	hP8	$P6_3/mmc$	D0$_{19}$
γ (TiAl)	tP4	P4/mmm	L1$_0$
O$_2$ (Ti$_2$AlNb)	oC16	Cmcm	
τ (Ti$_4$Al$_3$Nb, $ω_0$	hP6	$P6_3/mmc$	B8$_2$
σ (Nb$_2$Al)	tP30	$P4_2/mmm$	D8$_b$

As mentioned above, Nb is significantly soluble in comparatively large amounts in the γ phase as well as in the $α_2$ phase and has been found to be particularly advantageous for γ-TiAl alloys. The Ti-Al-Nb phase diagram is complicated because several ternary compounds with compositions not far away from the α+γ+β (B2) and $α_2$+γ+B2 three phase fields occur, which confirms that the constitution of the ternary Ti-Al-Nb system is depicted for the temperatures and compositions shown in Figure 2.14 and 2.15. The isothermal and vertical sections that are shown were taken from the most recent thermodynamic re-evaluation of Ti-Al-Nb and the constituent binary systems, conducted by Witusiewicz et al. [33].

However, Djanarthany et al.[36] have reported on the use of alloying additions to improve the mechanical properties and chemical properties of gamma titanium aluminides. In their study, the compositions studied can be classified into three groups designated as X_1, X_2, and X_3 with the relation to the compositions added to the two-phase ($α_2$+γ) alloys given as: Ti-(45-49)Al-(1-3)X_1-(1-4)X_2-(0,1-1)X_3. The X_1 group of

elements was significant for increasing the ductility; additions of 1-3 at.% V, Cr, Cr+Mn or V+Cr to Ti-48Al based alloys can enhance the room temperature ductility. Manganese additions were found to affect the ductility as confirmed by the activation of deformation in the γ phase. The X_2 group of elements was able to improve the oxidation resistance and strength, with additions of 2 at.% Nb. The X_3 group of elements only required the use of small additions to confer different properties in the alloys; this depended on the nature of the specific elements used, where C and N were able to improve the creep resistance, Si was found capable of yielding improvements in oxidation and creep resistance, and W was able to improve creep resistance in the temperature range of 550-850°C. Moreover, Huang and Chin [37] explained the guidelines in alloy design toward achieving desired properties, as follow. Generally, a reduction in aluminum content tends to increase strength level but reduces ductility and oxidation resistance. Additions of Cr, Mn and V to a maximum of 2 at% (for each element) have been shown to enhance ductility. Additions of 1–2 at% Nb are required to achieve sufficient oxidation resistance; additions of W, Mo, Si, and C to a maximum of 0.2–2 at% (for each element) can impart improvements in creep resistance. Additions of B from 0.2–2 at% act as a grain refining coagulant and are used for stabilizing the microstructure during high temperature service. Additionally, the degree of grain refinement and mechanical properties that can be achieved by boron additions also appear to be dependent on Al content and cooling rate that occurs in the high-temperature phase field. For the case of phase transformations in several TiAl-based alloys, Hu and Botten [38] suggested the solidification sequence of the Ti-46Al-2Nb-2Cr-1B, Ti-48Al-2Nb-2Cr-1B, Ti-48Al-2Nb-2Cr, Ti-46Al-4Nb-4Hf-0.1Si-1B and Ti-44Al-4Nb-4Zr-0.2Si-0.3B, which represents the different sequences of phase

transformations that occur during equilibrium upon cooling, given as follow: the first three alloys, which contain 2Nb-2Cr, transform in the following two sequences upon cooling from the liquid. For the alloy containing 46Al, the sequence is $L \rightarrow \beta + L \rightarrow \beta \rightarrow \beta + \alpha \rightarrow \alpha \rightarrow (\alpha + \gamma) \rightarrow (\alpha_2 + \gamma)$. For the alloy containing 48Al, the sequence is $L \rightarrow \beta + L \rightarrow \beta + L + \alpha \rightarrow L + \alpha \rightarrow \alpha \rightarrow (\alpha + \gamma) \rightarrow (\alpha_2 + \gamma)$. Based on this, the first phase to form upon solidification in the alloy containing 46Al is, as shown above, a β-phase. However, in the case of the alloy containing 48Al, virtually no β-phase is formed, and the first phase to be formed is effectively an α-phase.

2.3 Phase transformations in γ-TiAl alloys

2.3.1 Solidification microstructures

Microstructures are significant factors to consider when determining the properties of gamma titanium aluminides. Thus, the melting and subsequent solidification of alloys are important because they play a crucial role in determining the microstructures, the textures, the distributions of alloying elements in wrought or powder products. The phase transformation process during solidification depends on thermodynamic equilibrium and is controlled by two processes; the driving force, and the complex heat transport and diffusion processes, which depend on the solidification conditions. Previous investigations on the characteristics of solidification microstructures based on Al concentration range for binary two-phase γ-alloys found that two peritectic reactions occur within a rather narrow concentration range, as shown in Figure 2.16[24], which results in the solidification process being highly sensitive to alloy composition. In a previously published work on solidification, McCullough et al. [21] investigated the

phase equilibria and solidification mechanisms in Ti-Al alloys and Ti-Al binary alloys in the range of 40–55 at.%Al. The primary solidification phase was identified by direct observation of dendrite symmetry, and the analysis of this phase was conducted with *in situ* high-temperature X-ray diffraction. The results of this study confirmed that a hexagonal close-packed α-phase exists close to the melting point of the alloys containing 46–50 at.%Al, while leaner alloys (<44%Al) were in a cubic β-phase field at similar temperatures. For alloys in the range of 40–49 at. %Al, β was found to be the primary phase in local equilibrium with the liquid, and from 49-55 at.%Al, α was the primary phase. The γ-segregate was first observed at 46 at.%Al, and its fraction increased with increasing Al content. Both β and α dendrites transformed in solid-state to a lath structure, which consisted of layers of α_2 and γ. The growth direction of β dendrites was found to be $\langle 100 \rangle$ with an alignment parallel to the heat-flow direction, whereas α dendrites grew in the [0001] with dendrite side arms along the $\langle 1010 \rangle$. A revised phase diagram is proposed, for the composition range studied, to incorporate two peritectics (L+β→α and L+α→γ) with a high temperature α-phase field.

Muraleedharan et al., as cited in Appel et al. [24], presented a study on the texture of Ti-48Al-2Nb-2Cr cast alloys. The study found that, when the alloys were rapidly cooled during solidification, they revealed a lamellar microstructure with $\langle 111 \rangle$ directions of the γ phase, parallel to the growth direction of the columnar grains. This confirmed the growth of the α dendrites on the [0001], parallel to the heat flow direction; γ lamellae were also formed, and according to the Blackburn-orientation relationship [39] their orientation is given as $(0001)_{\alpha 2} \| \{111\}_{\gamma}$ and $\langle 11\bar{2}0 \rangle_{\alpha 2} \big\| \langle 1\bar{1}0 \rangle_{\gamma}$, which describes the crystallographic alignment of the γ lamellae with respect to the α_2 lamellae in the earlier

α grain. However, similar textures of the α grain growth along the [0001] direction were observed by Dey et al. [40] for a Ti-46.8Al-1.7Cr-1.8Nb (at.%) alloy. Further, Hu et al. [41] found that the growth direction of the α phase of the Ti-45Al-7Nb alloy was 80° from the $\langle 0001 \rangle_\alpha$ direction and approximately in the $\langle 11\bar{2}0 \rangle_\alpha$ direction.
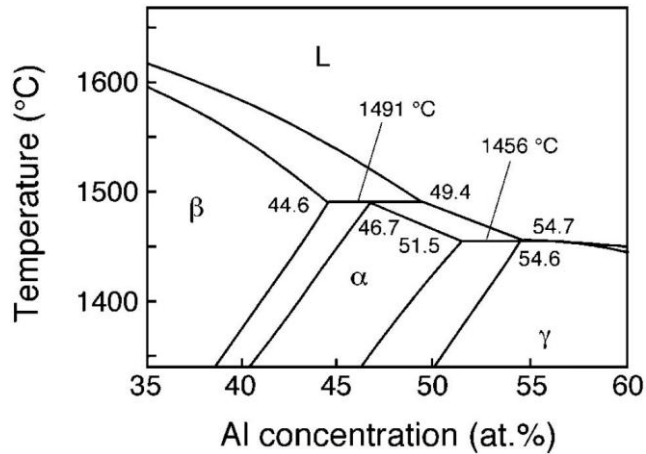

Figure 2.16 A section of the calculated binary Ti-Al phase diagram according to the thermodynamic evaluation of Witusiewicz et al., as cited in Fritz Appel et al. [24].

In the study of Wittig [42], it was reported that the phase transformation of Ti-48Al-2Cr (at.%)alloy after splat quenching contained a massive phase of nucleatedα: the α grain boundaries were identified with an orientation relationship of $[111]_\gamma$ //$[0001]_\alpha$ and $\{110\}_\gamma$ //$\{1120\}_\alpha$. Nakai et al. [43] reported the orientation relationship of Ti-48at.%Al obtained by rapid cooling; it was found that the retained regions decomposed into the $(\alpha_2 + \gamma)$ lamellar structure (LS), which exhibited similar characteristics to those in the Ti-40 at.%Al alloys. Both the fine Widmanstätten γ structure (FWS) and the Widmanstätten γ structure (WS) form in the α phase with the Blackburn orientation

relationship, $(0001)_\alpha \| \{111\}_\gamma$ and $\langle 2110 \rangle_\alpha \| \langle 110]_\gamma$; and the habit planes are $\{111\}_\gamma \| \{0111\}_\alpha$. The formation of the massive α, the FWS and the WS is suppressed by increasing the degree of order while α phase matrix transforms into the α_2 phase.

From the Blackburn orientation relationship, Yamaguchi and Umakoshi [44] suggested that the structure results from the growth of $L1_0$-TiAl on the basal plane of DO_{19}-Ti$_3$Al. However, because the different $\langle 110 \rangle$ directions on the (111) plane within the $L1_0$ structure are not equivalent (due to the stacking of alternate layers of Al and Ti atoms perpendicular to the c-axis); however, the $\langle 11\bar{2}0 \rangle$ directions on the (0001) plane of the DO_{19} structure are identical, such that TiAl forming on the basal plane of Ti$_3$Al can do so in any of six different orientations: $[\bar{1}10]\|[11\bar{2}0]$, $[\bar{1}10]\|[1\bar{2}10]$, $[\bar{1}10]\|[\bar{2}110]$, $[1\bar{1}0]\|[11\bar{2}0]$, $[1\bar{1}0]\|[1\bar{2}10]$, and $[1\bar{1}0]\|[\bar{2}110]$. Zambaldi [45] further investigated the previous works of Inui et al. [46], Inui et al. [47], Inui et al. [48], Inui et al. [49], and Inui et al. [50], which were carried out on the domain structure of γ-TiAl with a focus on the orientation relationships between the six orientation variants in γ-TiAl in Figure 2.17; based on the results, Zambaldi[45] explained that the six orientation variants of the phase fall into two groups of three. Within these groups, the variants have mutually perpendicular c-axes. These variant triplets are called order variants. The order variants can alternatively be visualized as generated by a 120° rotation around the (111) plane normal. For the notation of γ/γ disorientations, it is sometimes useful to assume a cubic structure. The γ phase forms a domain structure of twin-related lamellae. However, due to the ordered structure, the fcc 60°-around-[111] twin type splits into three types. The first is a true or coherent 180°-around-[111] twin-relation, in which the intermetallic

order is not disturbed; the second is a ±60°-around-[111] pseudo-twin relationship, for which an order-fault is formed in addition to the change in stacking order. For the first case, which is a perfect twin relation, the projections of the c-axes onto the (111) interface are parallel to each other, as seen in Figure 2.17. The term 'pseudo-twin' boundary is derived from the notion that this type of boundary otherwise would simply be 60°-around-⟨111⟩ twin, if the intermetallic order as well as the tetragonal distortion of the lattice are ignored, i.e., as in the fcc case.
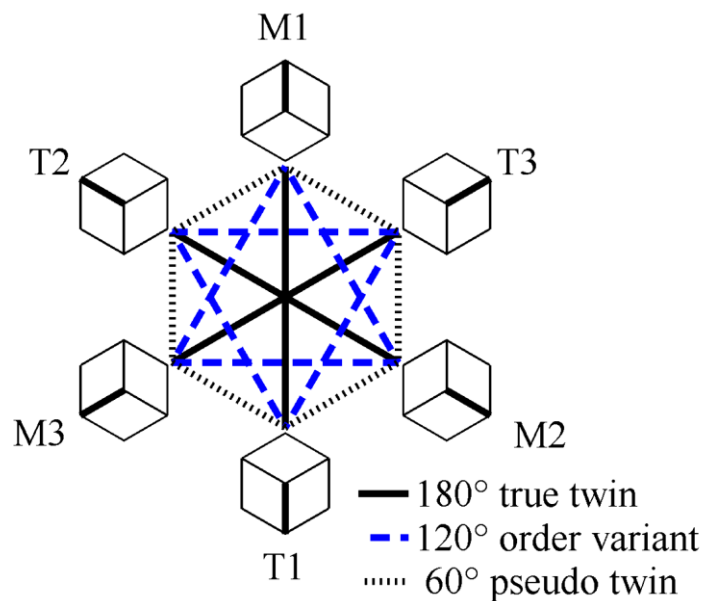

Figure 2.17 Orientation relationships between the six orientational variants in
γ-TiAl. The c-axis is emphasized. The opposing variants are in a true-
twin relationship, e.g., T1 and M1. The assignment of the twin (T) and
matrix (M) labels is arbitrary. In the presence of the α_2-phase, the
$(0001)_{\alpha2}$ basal plane will be parallel to the plane of illustration. [45]

Yamamoto et al. [51] classified the γ/γ interfaces into three types: the variant interface, the perfect-twin and the pseudo-twin boundaries. The variant interfaces become extinct while the perfect-twin boundaries increase drastically during the early stage of aging. Under this classification, which is summarized in Figure 2.18, the atoms are arranged on

the {110} planes for all three types of γ/γ interfaces. The perfect-twin exhibits an exact mirror image across the interface, even with respect to the atomic type, whereas the pseudo-twin only has a quasi-mirror image, in which different atomic configurations are present due to its ordered structure. The variant has the same lattice configuration but a different sub lattice configuration on both sides of the interface.
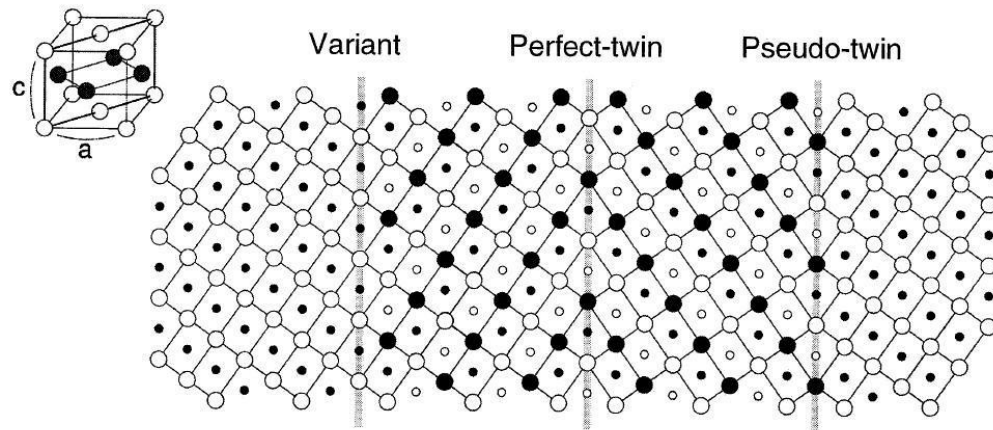

Figure 2.18   Atomic configuration of the {110} planes, showing the three types of interfaces in the L1$_0$ structure. (The small circles represent the atomic positions on the plane, while the large circles are used to represent atomic positions above or below the plane. The solid and open symbols refer to the a- and b-sublattices in the L1$_0$ plane.) [51]

2.3.2 Solid state transformation

Studies on the phase transformation in solid state gamma titanium aluminides have focused on the behavior of high temperature disorder, finding that the α-single phase field depends strongly on the cooling rate. In a study on the phase transformation of γ-TiAl-based alloys, Denquin and Naka [52] explained the formation of γ-TiAl from two possible pathways, (i) $\alpha \rightarrow \alpha_2' \rightarrow \alpha_2 + \gamma$ and (ii) $\alpha \rightarrow \alpha_2 + \gamma$; in either case, upon cooling, the α phase undergoes an ordering reaction into the α$_2$ phase. A fully lamellar

structure was observed in both the α+γ and α_2+γ phase fields, and the whole sequence of lamellar formation involves (i) a crystal structure change from hcp to fcc, (ii) a chemical composition change through atom transfer, and (iii) an ordering reaction of the FCC structure, which leads to the final $L1_0$-γ phase. The orientation relationships between the fcc lattice-based phase and the hcp lattice-based phase were found to be $(0001)_{\alpha2}\|\{111\}_{\gamma}$ and $\langle 11\bar{2}0\rangle_{\alpha2}\|\langle 1\bar{1}0\rangle_{\gamma}$. A mechanism of lamellar structure formation was proposed by Yang and Wu [53], who described the lamellar structure formation in a binary Ti-40 at.% Al (eutectoid composition), concluding that the order domain boundaries (ODBs) in γ lamellae are related to that of the anti-phase boundaries (APBs) in the α_2 matrix, which are introduced during a prior $\alpha \rightarrow \alpha_2$ ordering event. During the formation of a γ lamella, the propagation of Shockley partials across a pre-existing α_2 APB induces the formation of an ODB, which separates the two distinctly oriented γ domains. However, this mechanism does not explain the presence of ordered domains in the γ lamellae formed in the two-phase α+γ field. Denquin and Naka [52] reported that the α_2-APBs are formed during quenching, while the formation of γ domains takes place before quenching; this means that the α_2-APBs are not responsible for the formation of ordered domains in γ because the size of the γ domains is much larger than that of the anti-phase domains present inside the α_2 lamellae after quenching from the α+γ field. Denquin and Naka [52] also explained the formation mechanism of the γ lamellae, proposing the schematic shown in Figure 2.19; they found that, if the c-axes do not coincide, both ordered domains in a given lamella result in the formation of ODBs. Otherwise, such an encounter can be perfect or produce an APB. It is worth remembering here that, during the thickening process, the encounter of two lamellae can also result in the formation of twin boundaries (TBs) or pseudo-twin boundaries (PTBs),

if their (111) stacking sequences are different. It should be noted that a PTB is a combination of a TB with an ODB.
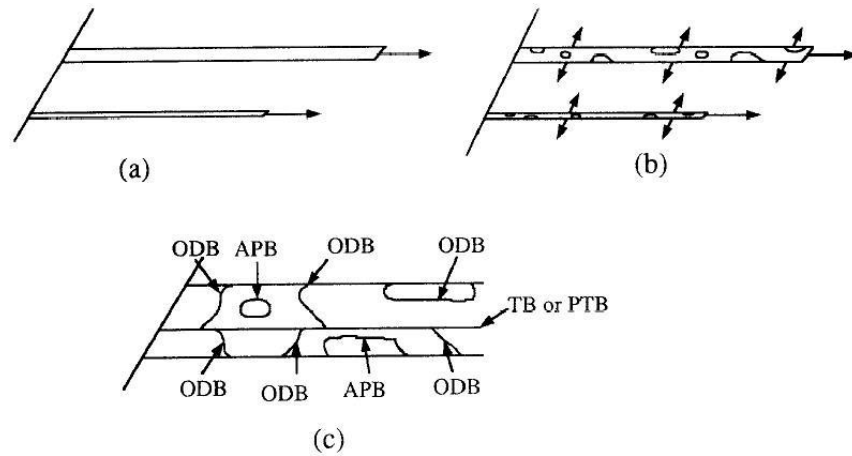

Figure 2.19 A schematic representation of the formation sequence of γ lamellae [50]

Figure 2.19 demonstrates (a) the propagation of Shockley partial dislocations, which give rise to a local FCC-type structure, and (b) the nucleation of orientation variants at a number of separate sites in the metastable FCC-type structure. It should be noted that this ordering reaction takes place during the growth and coarsening of the lamellae. Additionally, Figure 2.19 depicts (c) the encounter of the orientation variants after their growth, which leads to the formation of order domain boundaries (ODBs) as well as to the formation of anti-phase boundaries (APBs) in a given lamella. Coarsening of the lamellae leads also to the formation of twin or pseudo-twin boundaries (TBs or PTBs).

Zghal et al. [54] studied the microstructural characteristics of a fully lamellar Ti49Al47Cr2Nb2 alloy and suggested three sequences of lamellar transformation, identified in order of decreasing temperature: (i) a high-temperature heterogeneous transformation characterized by the nucleation of isolated primary γ lamellae mostly belonging to the same orientation group and having the same local order; (ii) a low-

temperature homogeneous transformation in the ordered α_2 phase characterized by the formation of a fine lamellar structure with an even distribution of the orientation groups and a random ordering of γ lamellae; and (iii) a coherent interfacial transformation at the α_2/γ interfaces characterized by the nucleation of ultra-fine twin related lamellae.
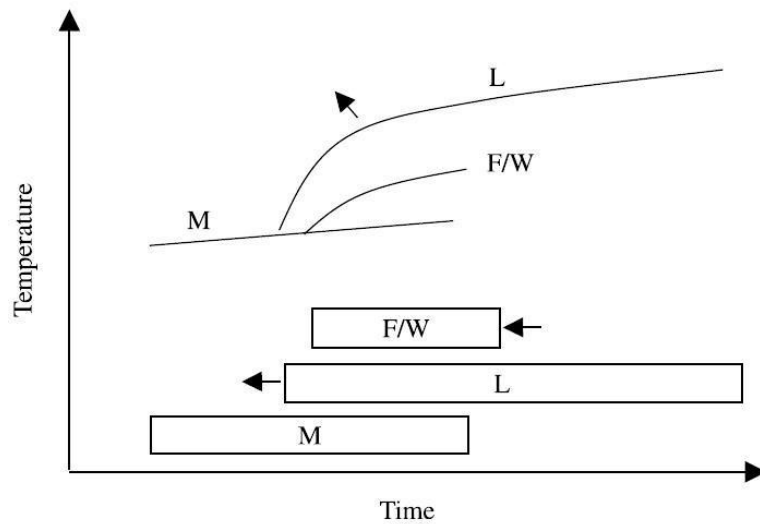

Figure 2.20 Schematic illustration showing the effect of grain size on the CCT curves and regimes of TiAl-based alloys. M stands for massive, L for lamellar and F/W for feathery/Widmanstätten transformations. The arrows show the directions of shifting in regime boundaries and curves caused by grain refinement. [55]

Hu and Botten [38] reported CCT and TTT diagrams for Ti-46Al-Nb-2Cr-1B, Ti-46Al-4Nb-4Hf-0.1Si-1B and Ti-44Al-4Nb-4Zr-0.2Si-0.3B and found that the massive transformation occurs at the highest cooling rates used $(500°C\ s^{-1})$ in all of the alloys studied, apart from Ti–44Al–4Nb–4Zr–0.2Si–1B and the high-temperature beta phase, which partially transformed during rapid cooling to a lenticular alpha; together, with the remaining beta, the lenticular alpha was retained at room temperature. Further, Hu et al.[55] and Saage et al. [56] summarized the possible microstructures that can result

from the use of different cooling rates after heating to the α-phase field; in this case, the results were based on the Jominy end quench test, which was successfully applied to the investigation of phase transformation kinetics in TiAl alloys shown, as shown in Figure 2.20 and 2.21.
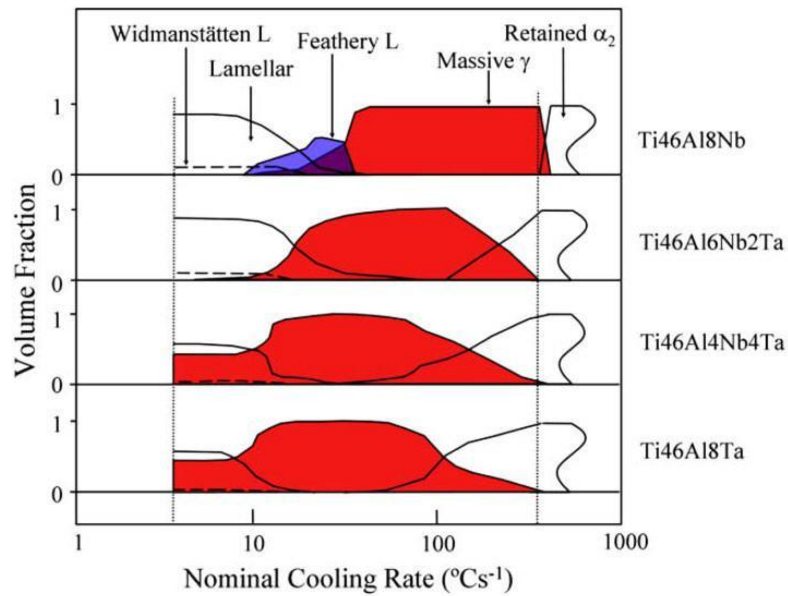
Figure 2.21 Jominy curves showing the relationship between the nominal cooling rates and the fractions of the various microstructures observed along the lengths of these samples [56].

Huang et al. [57] reported the phase transformation of Ti46Al8Nb (at%), cooled slowly from the alpha phase field to different temperatures within the alpha plus gamma phase field and then cooled rapidly to room temperature, using iced brine as the quenching medium. In the study, it was shown that the massively transformed gamma inherits (nucleates upon) the orientation of the lamellar gamma and is thus also incoherent with the surrounding alpha matrix. When massively transformed gamma nucleates on coherent defects, such as stacking faults or lamellae within grains, it also has no orientation relationship with the alpha phase, and thus, it forms a high-angle incoherent

boundary, which allows for rapid growth. The detailed observations are discussed in terms of the behavior of the factors that govern the nucleation of massive gamma and the propagation of the transformation front between the massive phase and the parent alpha. However, the authors explained in earlier publications (Hu et al. 2006 [55] and Saage et al. [56]) that there is a clearly discernible competition between the growth of lamellae and the growth of massive gamma under the cooling conditions used when attempting to refine microstructures. Massive gamma nucleates at the same cooling rate in all alloys but the window for growth is larger in samples alloyed with Nb or Ta, which are slow diffusers. Because the growth of massive gamma does not require diffusion but the growth of lamellae does, the mechanism of nucleation via lamellae can explain the influence of alloy content on the ability to transform samples through thickness at acceptably slow cooling rates.

2.3.3 Massive transformation

Massive transformation (MT) is a type of partionless transition that occurs during the cooling or heating of some crystalline materials. It involves a change in crystal structure without changing the composition from the parent phase to the product. Because the appearance of the product phase is always blocky or massive, such transition has received its name as the ''massive transformation.''

Hono et al. [58] investigated the ultrafine γ-lamellae that form in Ti-48 at.%Al, quenched into ice water from the single-phase α-field, and showed that ultrafine lamellae composed of $\alpha_2+\gamma$ phases were found surrounded by the massively transformed γ; additionally, they confirmed that these lamellar structures were produced

by the diffusional process. However, the compositions of aluminum in both α_2 and γ in the ultrafine lamellae were slightly higher than the equilibrium values, because the composition of each phase during the nucleation and growth stage is frozen in.
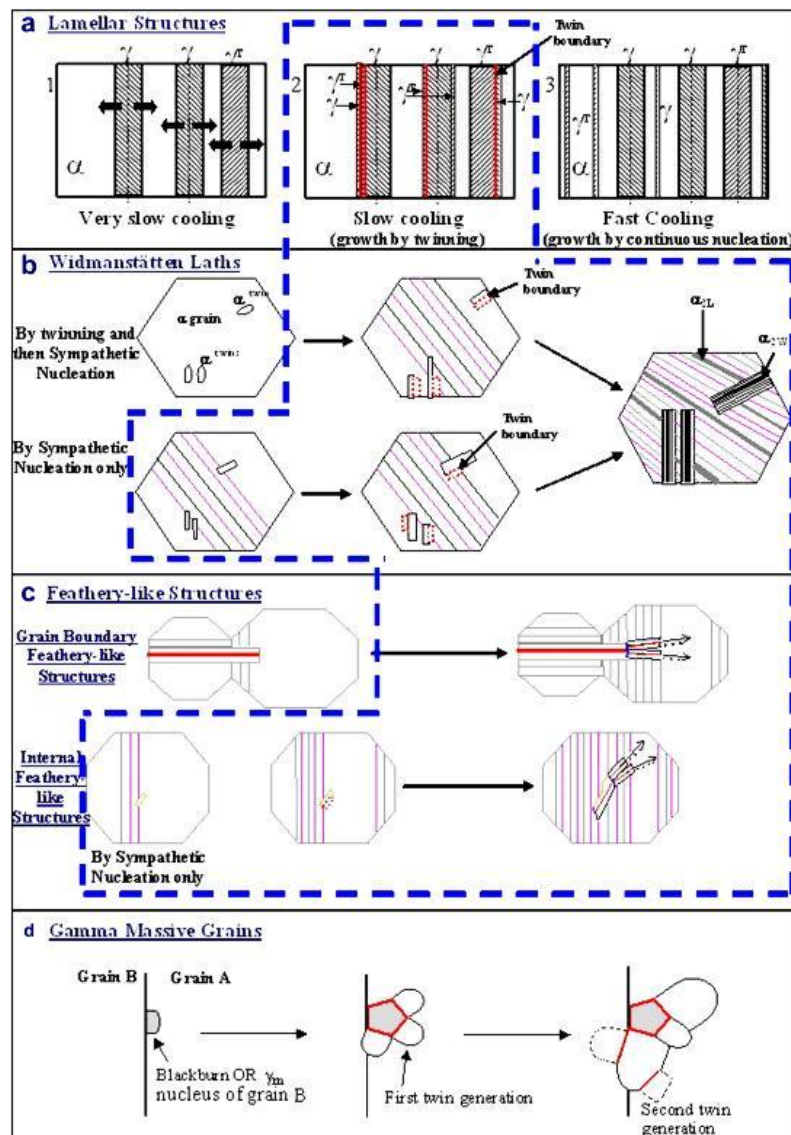

Figure 2.22 Schematic representation of possible development mechanisms of various structures generated during heat treatment of the $(\alpha_2 + \gamma)$ TiAl-based alloy from the high-temperature α domain. The marked region (bold dashed line) shows the domain under the influence of sympathetic nucleation.[40]

Correspondingly, Lefebvre et al. [59] studied the behavior of multicomponent alloys for the massive γ phase (γ_m) of binary Ti-48Al alloy by atom probe field ion microscopy (APFIM) and showed that α_2 plates can precipitate during or just after the massive transformation, within the γ_m phase. This precipitation event is thought to be induced by the presence of oxygen, which is rejected from the γ_m-phase during the massive transformation.

Sankaran et al. [60] studied the γ-massive nucleation in a near-γ TiAl alloy of Ti-45Al-7Nb-0.2C (at.%). The results are summarized for the nucleation and growth stages of the γ-massive transformation nucleation as follow: (1) the nucleation stage, in which all nuclei of γ-massive (γ_m) domains were systematically found to present a BOR (i.e., $(0002)_\alpha \| \{111\}_\gamma$ and $\langle 11\bar{2}0 \rangle_\alpha \| \langle 1\bar{1}0 \rangle_\gamma$) with one α grain (parent grain) and to develop in the other (host grain), which corresponds with the results reported in other references, i.e., [40], [61], and [62]. The nucleation sites and configurations have been identified and can be classified by the decreasing order of efficiency: (a) a triple junction; (b) a grain boundary whose plane is close to the basal plane of one of the neighboring α grains; and (c) a grain boundary for which one γ_m nucleus in BOR with one of the neighboring α grains has another $\{111\}$ plane closely parallel to the basal plane of the other α grain (secondary near-orientation relationship configuration). Triple junctions are the most favorable sites for nucleation due to (i) the higher loss of the α/α interface energy expected from the γ_m nucleation and (ii) the higher probability of fulfilling one of the nucleation criteria associated with configurations (b) or (c). (2) The growth of the massive structure was concluded to be the further growth of the γ_m phase, which is always proceeded by the successive twinning steps over the $\{111\}_\gamma$ planes;

consequently, each γ_m domain can be divided into a limited number of subdomains in which every single grain originates from the same nucleus through twinning. In a given subdomain, no twin relationship exists between grains of the same generation, which could explain some of the inconsistency present in the literature regarding the crystallography of the γ_m phase. However, Dey [40] clearly explained the phase transformation from the high temperature α domain to produce lamellar, Widmanstätten, feathery ($\alpha_2 + \gamma$) structures, as well as the γ-massive phase transformation following the different cooling paths; their approach is summarized in Figure 2.22. The authors explained the results as follows: for a lamellar structure, the initial γ lamellae nucleate over the prior α/α grain boundary through heterogeneous nucleation; stress can be generated in the α grain due to the contraction associated with $\alpha \rightarrow \gamma$ phase transformation and/or to the pre-existing eigenstrains induced by the already transformed regions in the adjoining grains. The selection of a particular γ variant at the nucleation stage could be a mechanism for decreasing these internal stresses. After the primary nucleation of γ lamellae and during the lamellar growing stage, new γ lamellae nucleate over the lateral growing interfaces of the existing γ lamellae. Less energy is required for nucleation over the moving α/γ interface than inside the α matrix itself and, therefore, should be achievable for slowly cooled lamellar structures. Then, out of the possible three γ/γ interface types, the face-to-face true twin interface provides the minimum interfacial energy. Hence, the growth is more probable by the nucleation of another γ lamella with a face-to-face true twin relationship. The widths of the new γ lamellae remain thin because they nucleate later and at a lower temperature. This type of growth can be termed the "growth by twin generation." In contrast, the high degree of undercooling (sand cooling), i.e., a higher driving force, preferentially activates the

nucleation of new γ lamellae in the untransformed α phase grain boundaries, which can be termed the "growth by continuous nucleation." The $\gamma/\alpha_2/\gamma$ interfaces remained until the end, giving a higher amount of the α_2 phase and a lower number of the γ/γ interfaces in the sand-cooled specimen. Both types of growth are schematically represented in Fig. 2.23(a-2) and (a-3). With respect to Widmanstätten laths, Dey et al. [40] reported a summary of the specific crystallographic orientation relationships that occur between Widmanstätten laths and lamellar structures from the previous research of Dey et al. [61], Zhang et al. [63], and Hu et al. [64]. This summary defines the relationships as (a) between the α_2 phases of the Widmanstätten laths and the lamellar structure, which is approximately 65° around the $\langle 1\bar{1}00 \rangle_{\alpha 2}$ axes and is related to the hexagonal twinning system ($\{11\bar{2}2\}\langle\overline{11}23\rangle$) in the prior α phase. Earlier, this α_{2W}/α_{2L} 65° (α_2-Widmanstätten denoted as α_{2w} and the α_2-Lamellar denoted as the α_{2L}) misorientation and (b) between the γ laths of the Widmanstätten laths and the lamellar structures, which is approximately 50° around the $\langle 110 \rangle_\gamma$ axes. This minimum angular rotation is close to the Σ11 coincidence site lattice (CSL) boundaries (approximately 50.48° around the $\langle 110 \rangle_\gamma$ axes). The developmental mechanisms of Widmanstätten laths were explained by Dey et al. [40]: the nucleation of Widmanstätten laths occurs with a specific misorientation with respect to the host lamellar structures. This misorientation, when it is expressed for the fcc γ phase, is approximately 50° around the $\langle 110 \rangle_\gamma$ axes and corresponds to a Σ11 CSL boundary, and when it is expressed for the hcp α_2 phase, is approximately 65° around the $\langle 1\bar{1}00 \rangle_{\alpha 2}$ axes and corresponds to a twin. This indicates two possible types of nucleation mechanisms. One is that the first Widmanstätten lath might nucleate directly over the face of the existing γ lamellar structure with a 50.48° misorientation, which corresponds to an "edge-to-face Σ11 CSL

relationship." Another mechanism could be a twinning event ($\{11\bar{2}2\}\langle\bar{1}\bar{1}23\rangle$) in the high-temperature hexagonal grain induced by cooling, which is further transformed into the first γ Widmanstätten lath. The majority of Widmanstätten lath was grown from the face-to-face γ/γ twin relationship (true twin and pseudo-twin both) of the lateral interfaces and the occurrence of interfacial germination over the flat lateral faces of the initial γ Widmanstätten lath, which mostly maintains the face-to-face Σ3 CSL (60° around the $\langle 110\rangle_\gamma$ axes) twin relationship. The specific twin-related γ variants in the adjoining γ lamellae provide low interfacial energy, and therefore, the twin γ/γ interfaces with Σ3 CSL boundaries are favored. Finally, the α_2 phase is proposed to form by subsequent precipitation along the interfaces of the already formed γ laths. For the formation of the rapidly cooled Feathery-like structure, which Veeraraghavan et al.[65] define, the morphology is a fanning-out type of growth, consisting of misoriented lamellar packets. Dey et al. [66] classify the Feathery-like structure into two types of Feathery-like structures (γ_f); the γ_f–structures attached to a grain boundary will henceforth be denoted as the "$\gamma_{f\text{-}gb}$ structures" while the γ_f structures found inside a grain will be referred to as the "$\gamma_{f\text{-}int}$ structures," as shown in Figure 2.23. In their conclusions of the phase transformation procedure, Dey et al. [40] denoted that the $\gamma_{f\text{-}gb}$ structures produced during rapid cooling are γ lamellae of the neighboring grain's lamellar structure, which enter the empty adjacent α grain without any deviation. In the meantime, the entered lamellae also grow laterally, often nucleating other lamellae over the growing lateral side (face-to-face), mostly with the twin relationship (Σ3 CSL boundaries), and creating a packet (domain). As the lamellae continue to grow inside the adjacent α grain, they face more resistance in the form of elastic strain. This elastic strain is increased at the edges so the new lamellae nucleate with slight misorientations

over the edges of the existing lamellae. These small misorientations, which occur between the edges nucleated lamellae, can be as great as 15° and share the Σ1 CSL edge-to-edge orientation relationship. Again, new lamellae start nucleating over the lateral faces of these slightly misoriented lamellae through face-to-face Σ3 CSL and create another γ_f packet. The development of many γ_f packets ultimately generates the $\gamma_{f\text{-}gb}$ structures. Hence, all of the new lamellae, while growing laterally, generate packets through face-to-face Σ3 CSL, and while growing longitudinally, the lamellae create other lamellae through edge-to-edge Σ1 CSL. For the $\gamma_{f\text{-}int}$ structures, the lamellae share similar internal features with the $\gamma_{f\text{-}gb}$ structures, which suggest that the growth mechanism of the lamellae into multiple packets should be the same. Therefore, the only difference between the two structures would be the nucleation of the first lamellae. In the case of the $\gamma_{f\text{-}int}$ structures, the first lamella nucleates over the face of a pre-existing lamella in the host lamellar structure, with an average 37° misorientation around the $\langle 110 \rangle_\gamma$ axis (36.9° around the $\langle 100 \rangle$ axis - Σ5 CSL boundary relationship), which maintains the edge-to-face Σ5 CSL, as shown in detail in Figure 2.22(c).
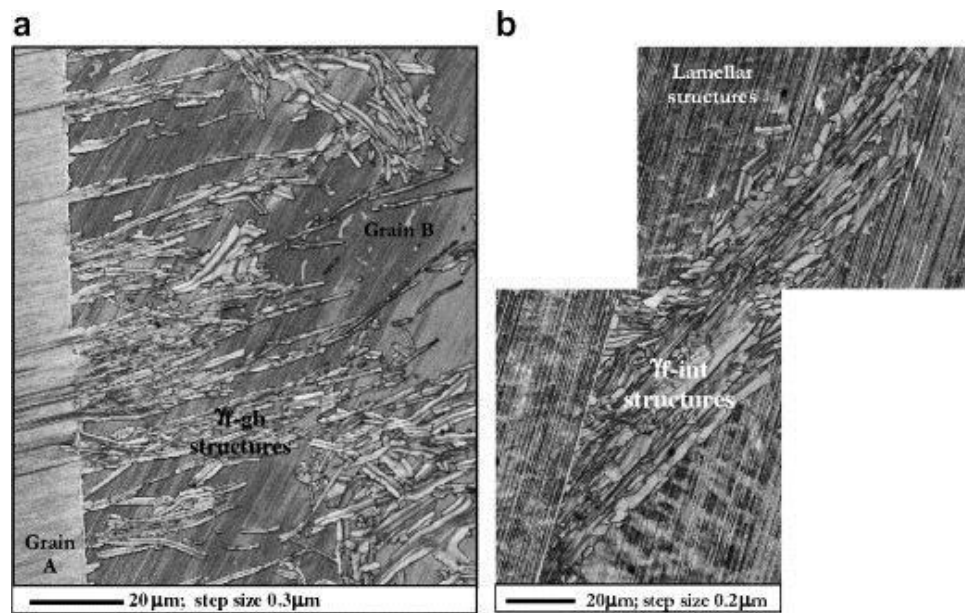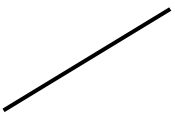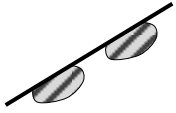

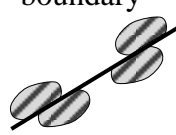**Figure 2.23** Optical micrographs of (a) the $\gamma_{f\text{-}gb}$ and (b) the $\gamma_{f\text{-}int}$ structures [40]

For the gamma-massive structure (γ_m), Dey et al. [40] divided the transformation of γ_m into nucleation and growth in Ti–46.8Al–1.7Cr–1.8Nb (at. %) alloy quenched with water and ice-water. Generally, γ_m grains nucleate heterogeneously over several sites, which are either α grain defects, like the triple junctions, grain boundaries, and twins inside the α grains, or the already existing γ grains. There are two possible cases for the γ_m phase transformation. In the first case, the γ_m nuclei were found to possess an exact BOR with one α grain or with α twin; however, in the second case, the γ_m nuclei were found to possess the same orientation as the existing γ grain. For the two cases above, these options can explain in detail the nucleation of the γ_m phase to produce γ_m nuclei, for which the preferred nucleation habit is over the α/α grain boundaries in the $(0002)_\alpha$ plane parallel to the $\{111\}$ plane of the γ nucleus; this minimizes the interfacial energy and superimposes or produces a minimum angle with respect to the α/α grain boundary plane, which is favored for nucleation. Sankaran et al. [60] found that that angle value in the case of the "fertile"grains (the grains associated with the effective nuclei) was lower than in the case of the 'sterile' grains (the grains without a nucleus), with a summary of the results given in Table 2.4. However, Dey et al. 2007 [66] studied massive γ grains that were generated in a Ti-46.8Al-1.7Cr-1.8Nb (at.%) TiAl-based alloy through ice-water quenching from α domain; in this study, they found that the γ_m nucleated by α_2 twins (K_1: $'\{\overline{2}12\overline{1}03\}'$, K_2: $'\{20\overline{2}1\}'$, η_1: $\langle 5\overline{1}46 \rangle$, η_2: $'\langle \overline{1}3\overline{2}2 \rangle'$ α_2 deformation twin) inside α grain in addition to other sites. The γ_m nuclei observed over the α_2 twin were found to have an exact BOR with the α_2 twin instead of with the α_2 matrix grain. Correspondingly, Dey et al. [61] and Dey et al. [66] concluded that the γ_m grains can also nucleate over the end regions (edges) of other structures, i.e., the lamellar structures, the Widmanstätten laths and the feathery-like structures. No specific

orientation relationship was described with respect to the α_2 matrix grain for the γ_m grains generated at the edges of the Widmanstätten laths and the feathery-like structures. Instead, the γ_m grains were revealed to exhibit a slight misorientation, which gave rise to the edge-to-edge $\Sigma 1$ CSL orientation relationship with respect to the Widmanstätten laths and the feathery-like structures (the grains were generated at their ends). For the growth of the γ_m phase, Dey et al. [67] explained that the γ_m grains always occurred only through the successive twinning of the different crystallographic equivalent {111} planes; that is, the γ_m nuclei produced new γ_m grains through {111} twinning. The twinning also continued, occurring in the newly formed γ_m grains, and this process produced several successive generations of γ_m grains [40].

Table 2.4 Different types of grain boundaries analyzed [60]

Type of grain boundary analyses	Type I: Grain boundary with no nucleus		Type II: Nucleus forming on the grain boundary		Type III: Nucleus forming on both sides of the grain boundary	
Number of grain boundaries analyses	41		41		9	
Angle between the GB trace and (0002) plane of α_2	θ_A	θ_B	θ_A	θ_B^*	θ_A^*	θ_B^*
Mean value	44.68	57.2	57.1	7.4	42.4	39.0
Mean ±standard Error		54.3±7.1		7.4±2.4		40.7±10.8

2.4 Effects of the alloying elements

Alloying elements are important for the improved properties of the gamma titanium aluminides. The effects of several investigated alloying elements can be explained as

follows. The alloying additions (B and C) used to obtain grain refinement for improved ductility of the lamellar structures has been investigated. Nb is the most likely candidate alloy for use in improving the high temperature resistance and promoting the massive transformation. For improved ductility at room temperature, Cr is the best alloying addition choice.

Yamaguchi et al. [68] reported the effect of Nb and C for Ti–45Al–8Nb–0.2C (in mol.%) alloy. They found that the Nb and C additions stabilize the lamellar microstructure because the α_2 to γ transformation proceeds by the migration of γ/α_2 lamellar boundaries, and the motion of ledges on the boundaries is a process of atomic migration. Nb atoms have a large size difference versus that of the Ti and Al atoms, which causes them to segregate to ledges along the γ/α_2 lamellar boundaries. The ledge mechanism involves two basic processes: the conversion of unit-height ledges (two atomic planes high) into multiple-height ledges (more than two atomic planes high) and the escape of unit ledges from multiple ledges. These processes take place at both the α_2/γ and γ/γ_s interfaces. It can be assumed that the ledge motion causes the transformations ($\alpha_2{\rightarrow}\gamma$ and $\gamma{\rightarrow}\gamma_s$)[69]. Nb has the lowest diffusivity among the major alloying elements investigated in both the γ-TiAl and α_2-Ti$_3$Al phases; Mishin et al. [70] explained that this is why Nb is likely to be a substitutional element that diffuses by the vacancy mechanism. Because the Nb atoms are considered to occupy the Ti sites in Ti$_3$Al, their diffusion is dominated by exchanges with vacancies on the Ti sublattice, and hence the larger effective activation enthalpy of Nb diffusion with respect to Ti self-diffusion implies a repulsive interaction between the Nb atoms and the Ti vacancy [71]. Therefore, additions of Nb reduce the mobility of ledges during the transformation [70]. Because the solubility limit of carbon is less in the γ phase than in the α_2 phase, the

excess carbon atoms also segregate to ledges along the γ/α_2 boundaries and have the net effect of reducing the minimum creep rate and retarding the creep acceleration in tertiary creep.

Moreover, Scheua1 et al. [72] evaluated the effect of Nb on the crystal structure. Their results revealed that, upon doping with Nb, the resulting structure can possess Ti and Nb atoms on the Al sites, which leads to a reduction in the c/a ratio of the tetragonal γ TiAl cell to approximately 1. However, in reality, the c/a ratio is increased compared to that of the binary phase, if the Nb atoms solely occupy the Ti sites and if Ti antisite defects (i.e., the Ti on the Al sublattice) are formed. Wang et al. [69] investigated the effects of Cr, Nb, Ta, W, Si on Ti47Al alloy. The results show that, at a given lamellar spacing, replacing 1 at.% Nb with 1 at.% Ta and replacing 0.2 at.% Ta with 0.2 at.% W induced an insignificant degree of change; however, additions of 0.3% Si decreased the creep resistance. Wang et al. [73] studied additions of W, B and Y in Ti–45Al–8.5Nb alloy. Their results showed that a uniform fully lamellar (FL) microstructure was observed in the center and at the rim of the different regions of the ingot following heat treatment; they also identified the presence of the β (B2) phase, borides and yttrium oxide in the FL microstructure as well as increased compression properties at elevated temperatures (approximately 1100 °C), which could be obtained without cracks even in engineering compression strains up to 80% for strain rates from 1×10^{-1} to 10^{-3} S^{-1}. Corresponding to these results, Zhang et al. [74] also found small amounts of the β phase as well as several boride rods and yttrium oxide precipitates in a fine-grained near lamellar structure of high-Nb content alloys (Ti–45Al–8.5Nb–0.2W–0.2B–0.02Y at.%).

However, Liu et al [75] suggested that the Nb and Al contents influence both the microstructure and yield strength of high-Nb content TiAl-based alloys with compositions in the range of 0–10 at.% Nb and 44–49 at.% Al. Their observations indicated that high levels of Nb solute in the γ-TiAl matrix lead to a high critical resolved shear stress (CRSS) of dislocation loops. High percentages of Nb additions also reduced the degradation rate of the fully lamellar microstructure following exposure at 1050 °C for 30 h. Both effects of the high Nb addition are related to the change in the directionality of Ti-Ti (Nb) and Nb-Al bonds within the lattice. The decrease in the Al content results in an increase in the volume fraction of the α_2 phase, which leads to a decrease in the lamellar spacing of the lamellar structure. The high temperature strength of the alloys is determined by the lamellar spacing (λ) as determined by the Hall–Petch equation ($k_\lambda \lambda^{-1/2}$).

For the effect of B on the gamma titanium aluminides, Li and Cao [76] presented the effect of 0.2 at.% boron additions on the phase transformations of Ti–47.5Al–2Cr–2Nb alloy during cooling from the α single phase field. They found that the boron additions promoted the formation of a fully lamellar microstructure during air cooling and oil quenching; they also found that the creep rupture life of the boron-modified alloy was two times longer than that of the boron-free alloy. Additionally, the boron additions raised the yield strength at room and elevated-temperatures and improved the ductility at room temperature.

For the effect of Mo, Qiu et al. [77] investigated the effect of Mo on Ti-45Al-xFe-yMo (x, y = 1, 2, 3, 4) alloys. Their results revealed that Mo shows a higher capability for stabilizing the β phase versus that of Fe; Mo was also found to induce very good hot

ductility at the elevated temperature. Correspondingly, Schmoelzer et al. [78] found that an increase in the Mo or Nb content increases the β/β_0-phase fraction as well as the eutectoid temperature.

Finally, Imayev et al. [79] reported their conclusions on an alloy design concept for the production of sound γ-TiAl+α_2-Ti3Al alloy castings with a chemically homogeneous and fine-grained microstructure. To produce this microstructure, they proposed a new concept, which was developed according to the following considerations: (i) solidification through the β phase to avoid the chemical inhomogeneities that results from the peritectic reactions and to form different orientation variants of the α phase from one β dendrite; (ii) an increase in the rate of heterogeneous nucleation of the α phase during the $\beta \rightarrow \alpha$ phase transformation owing to boron additions and a decrease in the growth rate of α due to niobium and molybdenum additions, which exhibit a low diffusive mobility; (iii) an increase in the stability of α grains against grain growth upon passing through the α single-phase field during cooling, which is attributed to the niobium, molybdenum, boron and carbon additions. The additions of niobium, and especially molybdenum, kinetically stabilized the β phase along α grain boundary and hindered the growth of α grain. The formation of borides might have been partially responsible for anchoring α grain boundary, as well. There are indications in the literature that additions of carbon also impede the growth of α grain because the carbon may segregate to α grain boundary. The obtained results also appear promising with respect to the development of new $\gamma + \alpha2$ alloys, which ideally will exhibit an improved workability as well as a favorable high-temperature behavior.